Progress of Theoretical Physics, Vol. 93, No. 1, January 1995

Clustering in Yrast States of ^{20}Ne Studied with Antisymmetrized Molecular Dynamics

Yoshiko KANADA-EN'YO and Hisashi HORIUCHI

Department of Physics, Kyoto University, Kyoto 606-01

(Received June 27, 1994)

Structure of the yrast line states of ^{20}Ne is studied with the Antisymmetrized Molecular Dynamics which is a method free from any model assumption such as the existence of clustering. The construction of the rotating intrinsic states is made by the frictional cooling method under the constraint that the expectation value of the angular momentum vector takes the given value in its magnitude while its direction is determined variationally. Angular momentum projection is applied to these rotating intrinsic states in order to get good angular momentum states. Two-body spin-orbit force is adopted and nucleon spin orientations expressed by spin coherent states are determined by energy variation, which enables us to describe the dissolution of clusters more satisfactorily. It is found that for both positive and negative parity low spin states, the two-cluster structure of $^{16}O+\alpha$ results as a predominant configuration and that the $^{16}O+\alpha$ clustering becomes weaker as the spin goes up and mixes with the spin-aligned oblate structure when going from 6^+ to 8^+. The yrast states with 10^+, 12^+ and 11^- are found to have the three-cluster-like structure composed of ^{12}C cluster and two α clusters.

§ 1. Introduction

In light nuclei the cluster structure is of fundamental importance as well as the shell-model-like structure (mean field structure).[2)~7)] It is generally expected that the clustering degree of freedom in the nucleus is activated more strongly as the excitation energy goes up, and that the nucleus can undergo the structure-change from the shell-model-like structure in the ground state energy region to the two-cluster structure and further to the three-cluster structure as the excitation energy increases.[8),9)]

In ^{20}Ne, it has long been discussed that the two-cluster structure of $^{16}O+\alpha$ appears predominantly already in the ground band and also more clearly in its inversion-doublet partner, the $K^\pi=0^-$ band upon the 5.78 MeV 1^- state.[10),3)] The predominance of the cluster structure instead of the shell-model-like structure in the ground band is rather exceptional from the molecular viewpoint expressed in the so-called Ikeda diagram[8),9)] and in fact in the other light nuclei such predominance of the cluster structure in the ground band is not experimentally supported except in very light nuclei such as ^{7}Li and ^{8}Be where the formation of the mean field is not firm. This exceptional character of ^{20}Ne ground band has been called the transient character from the shell-model-like structure to the cluster structure and has been studied by many authors.[11)~15),3)]

When studied in detail, most calculations have given the result that the $^{16}O+\alpha$ clustering of the ground band becomes weaker toward the band terminal 8^+ state. The weakening of the clustering is in two ways depending on adopted theoretical models. One is the shrinkage of the distance between the α cluster and the ^{16}O cluster which is called the anti-stretching effect[16),3)] and the other is the increase of the component with broken spatial symmetry,[15),3)] namely the dissolution of the α cluster

or the change of ^{16}O cluster.

In this nucleus of ^{20}Ne there have been observed several rotational bands in rather low excitation energy region and it has been discussed both experimentally and theoretically that the predominant configuration of the third $K^\pi=0^+$ band built upon the 7.19 MeV 0^+ state is the three-cluster-like structure of $^{12}C+\alpha+\alpha$.[17)~20),3)] If it is the case, the structure along the yrast line will change largely when going from 8^+ to 10^+ in such a way that the above-mentioned weak $^{16}O+\alpha$ clustering structure of the 8^+ state changes to the three-cluster-like structure of the 10^+ state.

The discussions given above on ^{20}Ne structure indicate that when we go up along the yrast line of ^{20}Ne, we observe very interesting features and changes of the yrast state structure which is due to the formation and dissolution of clusters. In order to study theoretically the formation and dissolution of clusters, it is desirable to use such theoretical framework that does not assume the existence of clusters. However in the theoretical studies on the clustering in ^{20}Ne reported until now, the authors had to introduce the postulated clustering configurations into the theory, such as the $^{16}O+\alpha$ and $^{12}C+^8Be$ configurations.

The purpose of this paper is to study the formation and dissolution of clusters in the yrast states of ^{20}Ne. For this purpose we use the Antisymmetrized version of Molecular Dynamics (abbreviated to AMD)[21)~27)] which is the theory free from any model assumptions and hence does not assume the existence of any clusters at all. By this study with AMD we expect to elucidate the following problems: (i) Does the ground band have the $^{16}O+\alpha$ structure predominantly? (ii) How is the structure-change of the ground band near the band terminal 8^+ state? (iii) How is the clustering in the negative parity $K^\pi=0^-$ band? (iv) Does the $^{12}C+\alpha+\alpha$ clustering structure appear in the yrast states with spins higher than 8? We have adopted an improved AMD framework which is important to study these problems about yrast line structure. Using the constrained frictional cooling method for the variational calculation, we construct the rotating intrinsic state with given magnitude for the angular momentum expectation value. An attractive character of our constrained frictional cooling method is that the expectation value of the angular momentum vector is constrained only in its magnitude while its direction is determined by the energy variation. The wave function with good angular momentum is constructed by the angular momentum projection applied to this rotating intrinsic state. Since in describing the dissolution of clusters the effect of the non-central nuclear force should be taken into account sufficiently, we use spin coherent state for each nucleon spin state determined so as to minimize the total energy.

This paper is organized as follows. In the next section (§ 2) we explain the theoretical framework of AMD, namely the AMD wave function and the constrained frictional cooling method for the construction of the minimum energy state. In § 3 the two-nucleon force used in this paper is explained. In § 4 we give the calculated results and discuss the above-mentioned four problems. We will see that for both positive and negative parity low spin states, the two-cluster structure of $^{16}O+\alpha$ results as a predominant configuration and that the $^{16}O+\alpha$ clustering becomes weaker as the spin goes up and mixes with the spin-aligned oblate structure when going from 6^+ to 8^+. The yrast states with 10^+, 12^+ and 11^- are found to have the three-cluster-like

structure composed of ^{12}C and two α's. Finally in § 5 we give summarizing discussions.

§ 2. AMD wave function, constrained frictional cooling method and angular momentum projection

The AMD (Antisymmetrized version of Molecular Dynamics) is a theory which is applicable both to nuclear structure problems and to heavy-ion collision problems. Here we only explain the AMD framework for the sake of nuclear structure study. As for the AMD theory for the sake of nuclear reaction study the reader is referred to Refs. 24) and 25).

We describe the intrinsic state wave function of the system by a parity-projected Slater determinant whose single nucleon wave function is given by a Gaussian wave packet:

$$|\Phi^{\pm}(\{\boldsymbol{Z}_j, \xi_j\})\rangle \equiv (1 \pm P)|\Phi(\{\boldsymbol{Z}_j, \xi_j\})\rangle ,$$

$$|\Phi(\{\boldsymbol{Z}_j, \xi_j\})\rangle \equiv \frac{1}{\sqrt{A!}} \det[\varphi_j] , \quad \varphi_j \equiv \phi_{\boldsymbol{Z}_j} \chi_{\xi_j} \hat{\chi}_{\tau_j} ,$$

$$\langle \boldsymbol{r}|\phi_{\boldsymbol{Z}_j}\rangle = (2\nu/\pi)^{3/4} \exp\left[-\nu\left(\boldsymbol{r} - \frac{\boldsymbol{Z}_j}{\sqrt{\nu}}\right)^2 + \frac{1}{2}\boldsymbol{Z}_j^2 \right] \propto \exp\left[-\nu(\boldsymbol{r} - \boldsymbol{D}_j)^2 + i\frac{\boldsymbol{K}_j}{\hbar} \cdot \boldsymbol{r} \right] ,$$

$$\boldsymbol{Z}_j = \sqrt{\nu}\, \boldsymbol{D}_j + \frac{i}{2\hbar\sqrt{\nu}} \boldsymbol{K}_j , \tag{1}$$

where A is the total mass number, χ_{ξ_j} is the spin coherent state with a complex parameter ξ_j,

$$\chi_{\xi_j} \equiv \left(\frac{1}{2} + \xi_j\right)\chi_{\uparrow} + \left(\frac{1}{2} - \xi_j\right)\chi_{\downarrow} , \tag{2}$$

and $\hat{\chi}_{\tau_j}$ is the isospin state, $\hat{\chi}_p$ or $\hat{\chi}_n$.

The wave function $|\Phi(\{\boldsymbol{Z}_j, \xi_j\})\rangle$ of Eq. (1) is the same as the wave function of the Fermionic Molecular Dynamics proposed by Feldmeier.[28] Furthermore, $|\Phi(\{\boldsymbol{Z}_j, \xi_j\})\rangle$ can be regarded as a special case of the Brink-type cluster model wave function[29] where every cluster is composed of a single nucleon. When the parameters of the Brink-type wave function are treated as time-dependent parameters by using the time-dependent variational principle, the Brink-type cluster model is called the time-dependent cluster model (TDCM).[30] Therefore, $|\Phi(\{\boldsymbol{Z}_j, \xi_j\})\rangle$ can be also regarded as a special case of the TDCM wave function. The reason why we use the name AMD for our present approach to nuclear structure problems is mainly because of the following characteristic. Our approach is characteristic in the point that it is always combined with the frictional cooling method which determines the parameters of the wave function often under given constraints. Other characteristic points of our approach are the use of projection of parity and angular momentum and the frequent use of the superposition of Slater determinants. (In the case of heavy-ion collision problems, the AMD approach is characterized by its treatment of stochastic two nucleon collisions.) We give in the following the explanation of the frictional cooling

method.

In order to describe the structure-change along the yrast line, we construct the minimum energy state $|\Phi^{\pm}(\{Z_j, \xi_j\})\rangle$ under the constraint that the expectation value of the angular momentum vector by this state should be equal to the given value in magnitude. Namely we determine numerically the values of the parameters $\{Z_j, \xi_j, j=1\sim A\}$ which satisfy

$$\hat{E}\equiv\langle H\rangle\equiv\frac{\langle\Phi^{\pm}(\{Z_j,\xi_j\})|H|\Phi^{\pm}(\{Z_j,\xi_j\})\rangle}{\langle\Phi^{\pm}(\{Z_j,\xi_j\})|\Phi^{\pm}(\{Z_j,\xi_j\})\rangle}=\text{minimum}\,,$$

$$\hat{W}\equiv\hat{\boldsymbol{J}}\cdot\hat{\boldsymbol{J}}=\text{given value}\,,\quad \hat{\boldsymbol{J}}\equiv\langle\boldsymbol{J}^{\text{op}}\rangle\equiv\frac{\langle\Phi^{\pm}(\{Z_j,\xi_j\})|\boldsymbol{J}^{\text{op}}|\Phi^{\pm}(\{Z_j,\xi_j\})\rangle}{\langle\Phi^{\pm}(\{Z_j,\xi_j\})|\Phi^{\pm}(\{Z_j,\xi_j\})\rangle}\,, \tag{3}$$

where H is the total Hamiltonian operator and $\boldsymbol{J}^{\text{op}}$ is the total angular momentum vector operator. This constrained variational problem is solved by using the constrained frictional cooling method which we explain below.

First we choose the initial values of the parameters $\{Z_j, \xi_j, j=1\sim A\}$ arbitrarily or randomly under the constraint that the value of $\hat{W}$ $(=\hat{\boldsymbol{J}}\cdot\hat{\boldsymbol{J}})$ is equal to the given value. The state $|\Phi^{\pm}(\{Z_j, \xi_j\})\rangle$ with these initial parameter values is in general a highly excited state. We need to cool this initial state down to the minimum energy state keeping the value of $\hat{W}$ unchanged. It is achieved by solving numerically the following constrained frictional cooling equation for the parameters,

$$i\hbar\frac{d}{dt}u_k=(\lambda+i\mu)\left(\frac{\partial\hat{E}}{\partial u_k^*}+\eta\frac{\partial\hat{W}}{\partial u_k^*}\right), \tag{4}$$

where the variables $\{u_k, k=1\sim 4A\}$ stand for the variational parameters $\{Z_j, \xi_j, j=1\sim A\}$, and the multiplier function η which is real is determined by the condition

$$\frac{d}{dt}\hat{W}=0\,. \tag{5}$$

This constancy condition of $\hat{W}$ can be rewritten by using Eq. (4) as follows:

$$\begin{aligned}0&=\frac{d}{dt}\hat{W}=\sum_k\left(\frac{\partial\hat{W}}{\partial u_k^*}\frac{du_k^*}{dt}+\frac{\partial\hat{W}}{\partial u_k}\frac{du_k}{dt}\right)\\&=\sum_k\left[\frac{\partial\hat{W}}{\partial u_k^*}\frac{\mu+i\lambda}{\hbar}\left(\frac{\partial\hat{E}}{\partial u_k}+\eta\frac{\partial\hat{W}}{\partial u_k}\right)+\frac{\partial\hat{W}}{\partial u_k}\frac{\mu-i\lambda}{\hbar}\left(\frac{\partial\hat{E}}{\partial u_k^*}+\eta\frac{\partial\hat{W}}{\partial u_k^*}\right)\right]\end{aligned} \tag{6}$$

from which we get

$$\eta=-\frac{1}{2}\sum_k\left(\left(1+i\frac{\lambda}{\mu}\right)\frac{\partial\hat{W}}{\partial u_k^*}\frac{\partial\hat{E}}{\partial u_k}+\left(1-i\frac{\lambda}{\mu}\right)\frac{\partial\hat{W}}{\partial u_k}\frac{\partial\hat{E}}{\partial u_k^*}\right)\Big/\sum_k\frac{\partial\hat{W}}{\partial u_k^*}\frac{\partial\hat{W}}{\partial u_k}\,. \tag{7}$$

Cooling of the total energy is assured for arbitrary λ if μ is negative, because there holds the following relation,

$$\frac{d}{dt}\hat{E}<0\quad\text{for }\mu<0\,,\quad\lambda=\text{arbitrary}\,. \tag{8}$$

A proof of Eq. (8) is as below,

$$\frac{d}{dt}\hat{E}=\sum_k\left(\frac{\partial\hat{E}}{\partial u_k^*}\frac{du_k^*}{dt}+\frac{\partial\hat{E}}{\partial u_k}\frac{du_k}{dt}\right)$$

$$=\sum_k\left[\left(\frac{\hbar}{\mu-i\lambda}\frac{du_k}{dt}-\eta\frac{\partial\hat{W}}{\partial u_k^*}\right)\frac{du_k^*}{dt}+\left(\frac{\hbar}{\mu+i\lambda}\frac{du_k^*}{dt}-\eta\frac{\partial\hat{W}}{\partial u_k}\right)\frac{du_k}{dt}\right]$$

$$=\frac{2\mu\hbar}{\mu^2+\lambda^2}\sum_k\frac{du_k^*}{dt}\frac{du_k}{dt}-\eta\frac{d}{dt}\hat{W}$$

$$=\frac{2\mu\hbar}{\mu^2+\lambda^2}\sum_k\frac{du_k^*}{dt}\frac{du_k}{dt}$$

$$<0 \quad \text{for } \mu<0, \quad \lambda=\text{arbitrary}. \tag{9}$$

An attractive character of our frictional cooling method with the constraint on the magnitude $|\hat{\boldsymbol{J}}|$ of $\hat{\boldsymbol{J}}$ is that the direction of $\hat{\boldsymbol{J}}$ is not constrained but determined by the energy variation. This means that we do not impose such condition that $\hat{\boldsymbol{J}}$ is parallel to a principal axis of the intrinsic state. We will see later that actual calculations show the existence of the case where the direction of $\hat{\boldsymbol{J}}$ is tilted from the principal axes.

The minimum energy state $|\Phi^{\pm}(\{\boldsymbol{Z}_j, \xi_j\})\rangle$ obtained by the constrained frictional cooling method is a rotating (or cranked) intrinsic state of the yrast state and is not an eigenstate of the angular momentum. We construct the good angular momentum state $|\Phi^{\pm}_{KJM}(\{\boldsymbol{Z}_j, \xi_j\})\rangle$ by the projection method:

$$|\Phi^{\pm}_{KJM}(\{\boldsymbol{Z}_j, \xi_j\})\rangle\equiv P^J_{MK}|\Phi^{\pm}(\{\boldsymbol{Z}_j, \xi_j\})\rangle,$$

$$P^J_{MK}\equiv\int dad\cos\beta d\gamma D^{J*}_{MK}(\alpha\beta\gamma)\exp(-i\alpha\boldsymbol{J}_z^{\text{op}})\exp(-i\beta\boldsymbol{J}_y^{\text{op}})\exp(-i\gamma\boldsymbol{J}_z^{\text{op}}). \tag{10}$$

The three dimensional integration is made numerically. The principal axes of deformation are determined by diagonalizing the inertia tensor. In this paper we have not made the diagonalization with respect to the K quantum number, but we have selected such K quantum number that gives the minimum energy.

The AMD wave function can be extended from a single Slater determinant to a linear combination of Slater determinants:

$$|\Phi^{\pm}(\{\boldsymbol{Z}_j, \xi_j\}, \{\boldsymbol{Z}'_j, \xi'_j\}, \cdots, C, \cdots)\rangle=|\Phi^{\pm}(\{\boldsymbol{Z}_j, \xi_j\})\rangle+C|\Phi^{\pm}(\{\boldsymbol{Z}'_j, \xi'_j\})\rangle+\cdots. \tag{11}$$

All the discussions given above for the case of a single Slater determinant remain valid simply by replacing $|\Phi^{\pm}(\{\boldsymbol{Z}_j, \xi_j\})\rangle$ with $|\Phi^{\pm}(\{\boldsymbol{Z}_j, \xi_j\}, \{\boldsymbol{Z}'_j, \xi'_j\}, \cdots, C, \cdots)\rangle$ and by regarding the variational parameters as being given by $\{u_k\}\equiv(\{\boldsymbol{Z}_j, \xi_j\}, \{\boldsymbol{Z}'_j, \xi'_j\}, \cdots, C, \cdots)$.

The most important feature of the construction of the wave function in AMD with the frictional cooling method is that the wave function can be obtained without prejudice, i.e., free from any model assumption such as the existence of clustering. If the resulting wave function proves to have clustering structure, the existence of clustering can be insisted more convincingly than other usual cluster model studies. AMD is a new powerful method for the study of the formation and dissolution of clusters in nuclei.

§ 3. Two-body interaction and parameters

The interaction adopted in the Hamiltonian consists of three parts, central force, spin-orbit force and the Coulomb force. As the central force we used the Volkov No. 1 force[31] with the Majorana exchange mixture m being given by $m=0.6$.

As for the two-body spin-orbit force V_{LS} we adopted the G3RS force[32] expressed as

$$V_{LS}=\{u_I\exp(-\kappa_I r^2)+u_{II}\exp(-\kappa_{II}r^2)\}P(^3O)\boldsymbol{L}\cdot(\boldsymbol{S}_1+\boldsymbol{S}_2)\,,$$

$$\boldsymbol{L}\equiv\boldsymbol{r}\times\left(-i\frac{\partial}{\partial\boldsymbol{r}}\right),\quad u_I=-u_{II}=900\ \mathrm{MeV}\,,$$

$$\kappa_I=5.0\ \mathrm{fm}^{-2}\,,\quad \kappa_{II}=2.778\ \mathrm{fm}^{-2} \tag{12}$$

with $\boldsymbol{r}$ denoting the two-nucleon relative coordinate and with $P(^3O)$ denoting the projection operator onto the triplet odd (^3O) two-nucleon state. Since the effect of the spin-orbit force becomes rather appreciable in the ground band states near the band terminal 8^+ state, we have investigated slightly in detail the role of the spin-orbit force in this band terminal region by changing the strength u_{ls} ($u_{ls}\equiv u_I=-u_{II}$) of the spin-orbit force from the value of 900 MeV.

The Coulomb force was approximated by a sum of seven Gaussian functions as was done in the AMD calculations for heavy ion collisions in Refs. 24) and 25).

The oscillator parameter ν has been chosen for each constraint value of the angular momentum so that the energy expectation value by the rotating intrinsic wave function becomes minimum.

In this paper, for the sake of simplicity, we have fixed the nucleon spin orientations in treating the states other than the positive parity states with the angular momentum constraint $|\hat{\boldsymbol{J}}|\leq 8$. Namely in the case of these states, the ξ parameters have been fixed to be either $\xi=1/2$ or $\xi=-1/2$ which means we have adopted either $\chi_{1/2}=\chi_\uparrow$ or $\chi_{-1/2}=\chi_\downarrow$. Corresponding to this simplification, the angular momentum constraint has been made not for $|\langle\boldsymbol{J}^{\mathrm{op}}\rangle|$ but for $|\langle\boldsymbol{L}^{\mathrm{op}}\rangle|$ where $\boldsymbol{L}^{\mathrm{op}}$ is the orbital angular momentum vector operator. Hence in all the discussions given below for the states other than the positive parity states with $|\hat{\boldsymbol{J}}|\leq 8$, $\hat{\boldsymbol{J}}$ should be understood as expressing not $\langle\boldsymbol{J}^{\mathrm{op}}\rangle$ but $\langle\boldsymbol{L}^{\mathrm{op}}\rangle$.

§ 4. Results

4.1. *Density distribution and structure-change*

The value for the angular momentum constraint (Eq. (3)) has been given as follows:

$$|\hat{\boldsymbol{J}}|=J_c\,,\qquad(\hat{W}=\hat{\boldsymbol{J}}\cdot\hat{\boldsymbol{J}}=J_c^2)\,,$$

$$J_c=\begin{cases}0,2,4,\cdots & \text{for positive parity,}\\ 1,3,5,\cdots & \text{for negative parity.}\end{cases} \tag{13}$$

We use the notation $|\Phi^{(J_c)\pm}(\{Z_j, \xi_j\})\rangle$ for expressing the rotating (or cranked) intrinsic state obtained with the frictional cooling method under the constraint $|\hat{J}|=J_c$.

We naturally expect that the structure of the spin J state on the yrast line can be studied by analyzing the cranked intrinsic state $|\Phi^{(J_c=J)\pm}(\{Z_j, \xi_j\})\rangle$ obtained under the constraint $|\hat{J}|=J_c=J$. However, it is not necessarily true as we see later in § 4.4. We will see that in order to get the spin J state by the projection from $|\Phi^{(J_c)\pm}(\{Z_j, \xi_j\})\rangle$, the angular momentum constraint J_c in cranking should be rather smaller than J. Therefore we here caution the reader not to simply regard the properties of the rotating intrinsic state $|\Phi^{(J_c=J)\pm}(\{Z_j, \xi_j\})\rangle$ as directly representing the properties of the yrast state with the angular momentum J.

In order to discuss the deformation of the intrinsic states we introduce the principal X-, Y- and Z-axes determined by diagonalizing the inertia tensor $\mathcal{I}$ so as to satisfy $\mathcal{I}_{XX} \geq \mathcal{I}_{YY} \geq \mathcal{I}_{ZZ}$. The density distribution of the rotating intrinsic states without parity projection is shown in Fig. 1, where the density is integrated out along the X-axis and projected to the YZ-plane. We have found the deformation of $|\Phi^{(J_c)\pm}(\{Z_j, \xi_j\})\rangle$ is prolate for $J_c=0\sim6$ and oblate for $J_c\geq8$ in the case of positive parity states. For negative parity states it is also prolate for $J_c\leq7$, while it is neither

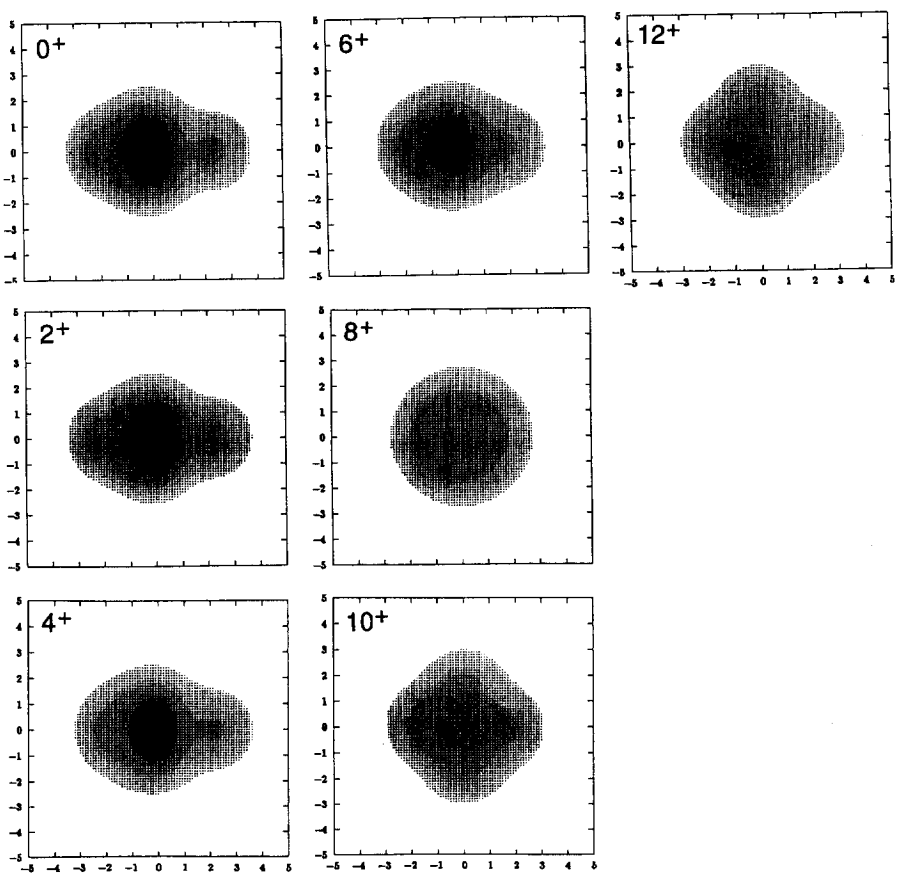

(a)

Fig. 1. (continued)

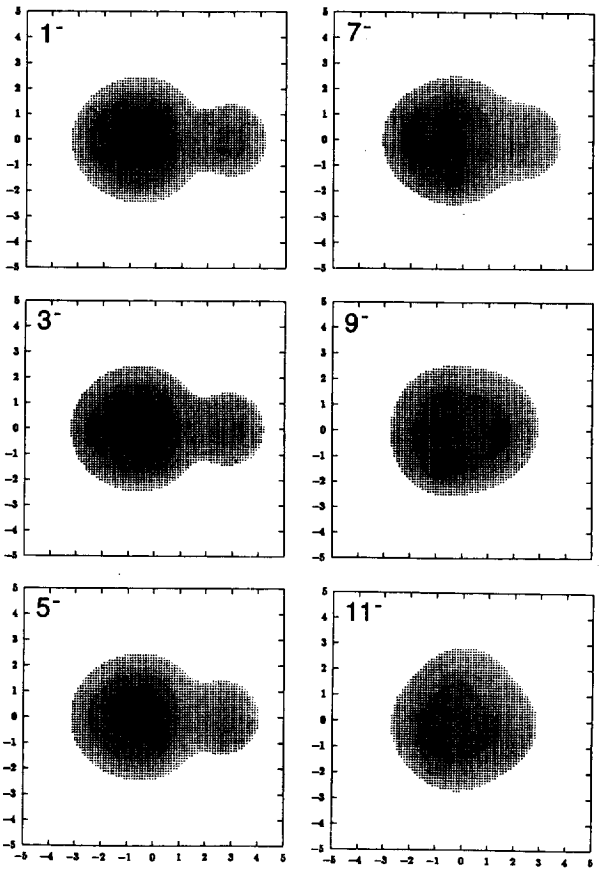

(b)

Fig. 1. The density distribution of the rotating intrinsic states without parity projection. It is integrated along the axis perpendicular to the plain. Units are in fm.

prolate nor oblate for $J_c=9$ and it is oblate for $J_c=11$. The deformed intrinsic states $|\Phi^{(J_c)\pm}(\{Z_j, \xi_j\})\rangle$ are all approximately axially symmetric except the states with $J_c=10$ and 12 of the positive parity and for $J_c=9$ of negative parity. We call the axis of approximate axial symmetry the symmetry z-axis which is chosen from one of three principal axes X, Y, Z. We show in Table I the calculated values of $\langle x^2\rangle$, $\langle y^2\rangle$, $\langle z^2\rangle$, and quadrupole moment $\langle(2z^2-x^2-y^2)\rangle$ in the intrinsic frame (principal axis frame), together with the optimum ν value of the rotating intrinsic states. Here, for example, $\langle x^2\rangle$ is defined by

$$\langle x^2\rangle \equiv \frac{\langle \Phi^{(J_c\pi)}(\{Z_j, \xi_j\})|(1/A)\sum_{j=1}^{A} x_j^2|\Phi^{(J_c\pi)}(\{Z_j, \xi_j\})\rangle}{\langle \Phi^{(J_c\pi)}(\{Z_j, \xi_j\})|\Phi^{(J_c\pi)}(\{Z_j, \xi_j\})\rangle}. \tag{14}$$

For the understanding of the detailed structure of the states $|\Phi^{(J_c)\pm}(\{Z_j, \xi_j\})\rangle$, we show in Fig. 2 the real parts of $\{Z_j\}$ which are the spatial centers of nucleon wave packets. For the states with the angular momentum constraint value $J_c=0\sim6$ for the positive parity and $J_c=1\sim7$ for the negative parity, four Z_j's locating at almost the same spatial point constitute an α cluster while the other 16 Z_j's constitute a compact

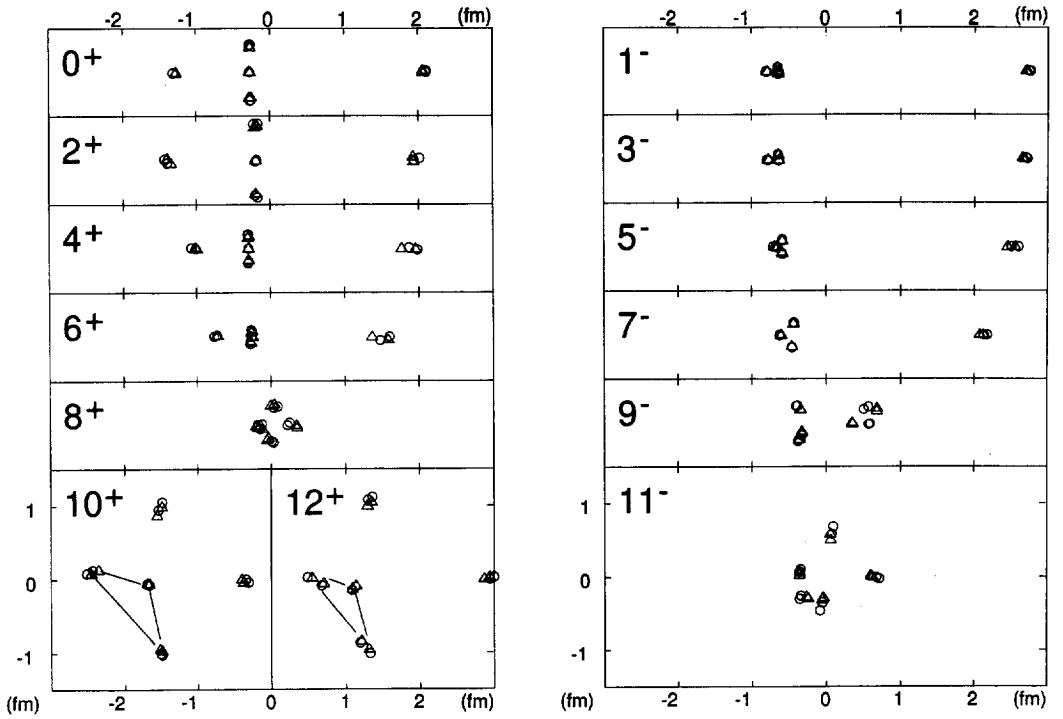

Fig. 2. The spatial centers $\{\boldsymbol{D}_j\}$ of nucleon wave packets. The circles correspond to protons and the triangles correspond to neutrons. In the cases of 10^+ and 12^+ three α clusters connected with lines form ^{12}C-like cluster.

tetrahedron of four α clusters and are almost equivalent to an ^{16}O cluster. We see that the distance between the α cluster and the ^{16}O cluster becomes smaller as the angular momentum constraint value J_c increases. This is the so-called anti-stretching effect mentioned in § 1. For the angular momentum constraint and parity $J_c^\pi=8^+$ and $J_c^\pi=9^-$, the α cluster is not recognizable. In the intrinsic states with higher angular momentum constraint values, we see two α clusters appear outside of a ^{12}C-like cluster composed of three α clusters forming a compact triangle.

As mentioned above the clustering feature becomes weaker as the angular momentum constraint J_c increases up to $J_c^\pi=6^+$ (7^-) for the positive (negative) parity mainly due to the anti-stretching effect. At the same time a little dissolution of α cluster is also seen in the states $|\Phi^{(J_c)\pm}(\{\boldsymbol{Z}_j, \xi_j\})\rangle$ with $J_c \geq 4$. This aspect is shown as the spatial dissolution of four $\boldsymbol{Z}_j$'s which compose an α cluster, and is considered to come from the effect of the two-body spin-orbit force. In fact the dissolution is never seen in the results with the spin-orbit force off. The breaking of the α cluster makes the energy higher due to the two-body central force while on the contrary it can make the energy lower due to the two-body spin-orbit force. It is expected that the latter gain of the energy often overcomes the former loss of the energy especially in the rotating intrinsic states with large J_c.

Another point to be discussed is the change of ^{16}O cluster. In all the positive and negative parity states with $J_c=0\sim7$, ^{16}O clusters are composed of four α clusters

Table I. The quadrupole moments and the optimum ν value of the rotating intrinsic states. The intrinsic z-axis is chosen to be the approximate axially symmetric axis.

J_c^π	$\langle x^2\rangle$	$\langle y^2\rangle$	$\langle z^2\rangle$	$\langle 2z^2-x^2-y^2\rangle$	$\nu(fm^{-2})$
0^+	28.2	28.2	58.6	60.8	0.245
2^+	28.0	28.1	56.5	56.9	0.250
4^+	28.9	29.4	56.0	53.7	0.235
6^+	29.6	31.3	50.4	39.9	0.230
8^+	39.4	39.2	31.7	−15.2	0.220
10^+	43.3	41.6	30.5	−23.9	0.230
12^+	48.3	43.4	31.6	−28.5	0.245
1^-	30.7	30.7	76.6	91.8	0.235
3^-	30.7	30.8	75.6	89.7	0.235
5^-	29.3	29.8	67.8	76.5	0.230
7^-	30.1	31.5	60.7	59.8	0.225
9^-	32.3	39.2	45.7	—	0.215
11^-	44.3	43.0	35.9	−15.5	0.205

forming a tetrahedron. Considering the size parameter ν of wave functions, an ^{16}O cluster is the p-shell closed state when the inter-α distance of tetrahedron is smaller than 1 fm. It is the case in the states except 0^+ and 2^+ states. However the state with $J_c^\pi=2^+$ has the biggest tetrahedron which is considered to have possible component of the excitation of ^{16}O cluster. It means that the core excitation of ^{16}O should be important for the low spin state in the positive ground band.

Here we caution the reader not to consider directly the shrinkage of the $\boldsymbol{Z}_j$'s locating region as the shrinkage of the density distribution of nuclear matter. In positive parity band, the $\boldsymbol{Z}_j$'s locating region seems to shrink also in the x and y directions as the constraint value J_c goes up to 6. However, the density distribution becomes larger in the directions of x and y axis due to the decrease of the size parameter ν of single particle Gaussian wave function. As seen in Table I, $\langle x^2\rangle$ and $\langle y^2\rangle$ tend to increase with J_c up to 6, which is consistent with the saturation property of nuclear matter.

We consider that the rotating intrinsic states $|\Phi^{(J_c)+}(\{\boldsymbol{Z}_j, \xi_j\})\rangle$ with $J_c\leq 8$ correspond to the experimental ground rotational band, while $|\Phi^{(J_c)-}(\{\boldsymbol{Z}_j, \xi_j\})\rangle$ with $J_c\leq 9$ correspond to the observed negative parity rotational band upon 5.78 MeV 1^- state. As mentioned in § 1, these two rotational bands have been regarded as constituting an inversion doublet, which is just supported by our results of rotating intrinsic states of positive and negative parities.

4.2. *Direction of the vector* $\hat{\boldsymbol{J}}$

The vector $\hat{\boldsymbol{J}}$ calculated with $|\Phi^{(J_c)\pm}(\{\boldsymbol{Z}_j, \xi_j\})\rangle$ (Eq. (3)) has been found, except for the negative parity intrinsic states with $J_c=9$ and 11, to be almost exactly parallel to the X-axis, which means it is perpendicular and parallel to the symmetry z-axis in the cases of prolate and oblate states, respectively. In the cases $J_c^\pi=9^-$ and 11^-, $\hat{\boldsymbol{J}}$ is slightly tilted from the principal X-axis. The angle θ between the vector $\hat{\boldsymbol{J}}$ and the X-axis is 8.8° for $|\Phi^{(J_c=9)-}(\{\boldsymbol{Z}_j, \xi_j\})\rangle$ and 4.1° for $|\Phi^{(J_c=11)-}(\{\boldsymbol{Z}_j, \xi_j\})\rangle$, while it is less than 1° for the other states.

The result that the vector $\hat{\boldsymbol{J}}$ is parallel to the X-axis suggests that the situation is similar to the rotation of a rigid body. The total energy of a rigid body rotating around a principal axis with given angular momentum J_c is the sum of the internal energy and the rotation energy $J_c^2/2\mathcal{I}$ with $\mathcal{I}$ standing for the moment of inertia around the principal axis. The lowest total energy under the given angular momentum is obtained by minimizing this rotation energy, which is achieved when the angular momentum vector (the rotation axis) is parallel to the X-axis with the largest moment of inertia.

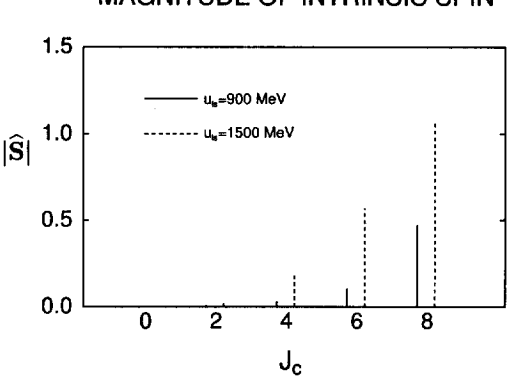

Fig. 3. The magnitude of the expectation value of the intrinsic spin angular momentum $\boldsymbol{S}^{\rm op}$ before total angular momentum projection. The solid line corresponds to the results with u_{ls}=900 MeV and the dashed line with u_{ls} =1500 MeV.

4.3. *Magnitude and direction of spin angular momentum vector* $\hat{\boldsymbol{S}}$

We have seen that in the rotating intrinsic state $|\Phi^{(J_c=8)+}(\{\boldsymbol{Z}_j, \xi_j\})\rangle$ the α cluster is not recognizable. In general we expect that in non-α-clustering states the effect of non-central force is stronger than in α-clustering states. Hence we expect that the magnitude of spin angular momentum $|\hat{\boldsymbol{S}}|$ is larger in $|\Phi^{(J_c=8)+}(\{\boldsymbol{Z}_j, \xi_j\})\rangle$ than in other $|\Phi^{(J_c)+}(\{\boldsymbol{Z}_j, \xi_j\})\rangle$ with $J_c \leq 6$, where $\hat{\boldsymbol{S}}$ is defined by the expectation value $\langle \boldsymbol{S}^{\rm op}\rangle$ as

$$\hat{\boldsymbol{S}}=\langle \boldsymbol{S}^{\rm op}\rangle \equiv \frac{\langle \Phi^{(J_c)+}(\{\boldsymbol{Z}_j, \xi_j\})|\boldsymbol{S}^{\rm op}|\Phi^{(J_c)+}(\{\boldsymbol{Z}_j, \xi_j\})\rangle}{\langle \Phi^{(J_c)+}(\{\boldsymbol{Z}_j, \xi_j\})|\Phi^{(J_c)+}(\{\boldsymbol{Z}_j, \xi_j\})\rangle},$$

$$\boldsymbol{S}^{\rm op} \equiv \text{spin angular momentum vector operator}. \tag{15}$$

We show in Fig. 3 the values of $|\hat{\boldsymbol{S}}|$ for $J_c=0\sim8$. We see clearly that $|\hat{\boldsymbol{S}}|$ for $J_c=8$ is much larger than those for $J_c=0\sim6$. Since the rotating intrinsic states with $J_c=0\sim6$ have α and ^{16}O clusters, the magnitude $|\hat{\boldsymbol{S}}|$ is expected to show the degree of the dissolution of clusters. The small $|\hat{\boldsymbol{S}}|$ seen in Fig. 3 shows that the dissolution of clusters is not so much in those states.

We define $\hat{\boldsymbol{L}}$ as the expectation value $\langle \boldsymbol{L}^{\rm op}\rangle$ of the total orbital angular momentum operator $\boldsymbol{L}^{\rm op}$ in the same way as $\hat{\boldsymbol{S}}$. Although the constraint in the variational calculation is only for $|\hat{\boldsymbol{J}}|=|\hat{\boldsymbol{L}}+\hat{\boldsymbol{S}}|=J_c$, the vector $\hat{\boldsymbol{S}}$ is found to be parallel to the vector $\hat{\boldsymbol{L}}$ for all the states with $J_c>0$ so that they satisfy $|\hat{\boldsymbol{L}}|+|\hat{\boldsymbol{S}}|=J_c$. The alignment of $\hat{\boldsymbol{S}}$ to $\hat{\boldsymbol{L}}$ has an important relation with the dissolution of α cluster in the states with large $|\hat{\boldsymbol{S}}|$ such as $|\Phi^{(J_c=8)+}(\{\boldsymbol{Z}_j, \xi_j\})\rangle$. The spin alignment in higher spin states of the ground band has been much discussed in shell model calculations[14] since long time ago.

4.4. *Energy*

We use the notation $|\Phi^{(J_c)\pm}_{KM}(\{\boldsymbol{Z}_j, \xi_j\})\rangle$ for expressing the state obtained by the angular momentum projection from $|\Phi^{(J_c)\pm}(\{\boldsymbol{Z}_j, \xi_j\})\rangle$;

$$|\Phi^{(J_c)\pm}_{KM}(\{\boldsymbol{Z}_j, \xi_j\})\rangle \equiv P^J_{MK}|\Phi^{(J_c)\pm}(\{\boldsymbol{Z}_j, \xi_j\})\rangle\,. \tag{16}$$

We have not made the diagonalization with respect to the K quantum number. Therefore we should make a suitable choice of "integration z-axis" which is the z-axis for the integration over Euler angles in angular momentum projection operator. We have made two choices: In one case the integration z-axis is chosen to be principal Z-axis which has the smallest moment of inertia $\mathcal{I}_{zz}$ and is perpendicular to the angular momentum vector $\hat{\boldsymbol{J}}$, and in another case it is chosen to be the principal X-axis which has the largest moment of inertia $\mathcal{I}_{xx}$ and is parallel to the angular momentum vector $\hat{\boldsymbol{J}}$. The K quantum number that gives the minimum energy after the angular momentum projection is found to be $K=0$ for the former choice of the integration z-axis and $K=J$ for the latter choice. To tell more in detail, in the case of the

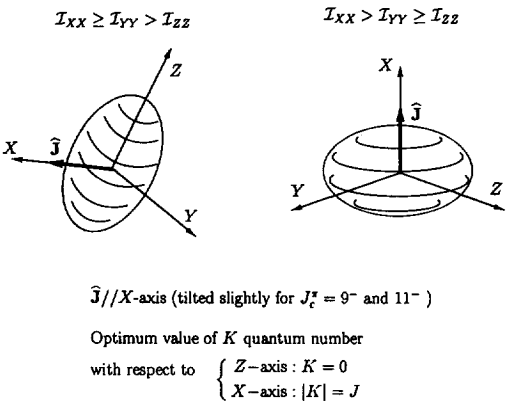

Fig. 4. Schematic picture for the understanding of the relation between the optimum value of K quantum number and the direction of the angular momentum vector $\hat{\boldsymbol{J}}$.

Table II. The squared amplitudes of the normalized projected components contained in the normalized intrinsic state. K_Z is the K quantum in the angular momentum projection with the principal axis Z about which quadrupole moment $\mathcal{T}_{zz}$ is the smallest. K_X is one with the principal axis X about which quadrupole moment $\mathcal{T}_{xx}$ is the largest.

		$\alpha^2(J_c, J)$				
J^π_c		$J=0$	$J=2$	$J=4$	$J=6$	$J=8$
0^+	$K_Z=0$	0.09	0.34	0.32	0.16	0.05
0^+	$K_X=J$	0.09	0.13	0.09	0.04	0.00
2^+	$K_Z=0$	0.07	0.28	0.29	0.17	0.06
2^+	$K_X=J$	0.07	0.15	0.16	0.10	0.04
4^+	$K_Z=0$	0.04	0.16	0.21	0.16	0.06
4^+	$K_X=J$	0.04	0.14	0.23	0.22	0.10
6^+	$K_Z=0$	0.01	0.04	0.09	0.14	0.11
6^+	$K_X=J$	0.01	0.05	0.16	0.33	0.31
8^+	$K_Z=0$	0.00	0.00	0.00	0.00	0.20
8^+	$K_X=J$	0.00	0.00	0.00	0.00	0.99
J^π_c		$J=1$	$J=3$	$J=5$	$J=7$	$J=9$
1^-	$K_Z=0$	0.22	0.34	0.26	0.12	0.04
3^-	$K_Z=0$	0.16	0.26	0.23	0.12	0.05
5^-	$K_Z=0$	0.08	0.14	0.16	0.12	0.06
7^-	$K_Z=0$	0.01	0.04	0.08	0.11	0.08
9^-	$K_Z=0$	0.00	0.00	0.00	0.02	0.10

principal Z-axis, the energies of the projected states with $K=\pm1$ are very close to the energy of the projected states with $K=0$, but the states with $K=\pm1$ are contained in the intrinsic state $|\Phi^{(J_c)\pm}(\{\boldsymbol{Z}_j, \xi_j\})\rangle$ only with very small amplitudes while the state with $K=0$ is contained with large amplitude. We show in Fig. 4 schematically the relation between the optimum value of the K quantum number and the direction of the angular momentum vector $\hat{\boldsymbol{J}}$. We denote $K=0$ with respect to the principal Z-axis as K_Z and $|K|=J$ with respect to the principal X-axis as K_X.

In Table II we give the squared amplitudes $a^2(J_c, J)$ of the normalized projected components $\mathcal{N}_J|\Phi^{(J_c)\pm}_{K_ZJK_Z}(\{\boldsymbol{Z}_j, \xi_j\})\rangle$ and $\mathcal{N}'_J|\Phi^{(J_c)\pm}_{K_XJK_X}(\{\boldsymbol{Z}_j, \xi_j\})\rangle$ contained in the normalized intrinsic state $\mathcal{N}|\Phi^{(J_c)\pm}(\{\boldsymbol{Z}_j, \xi_j\})\rangle$:

$$a^2(J_c, J)\equiv\begin{cases}\left|\dfrac{\langle\Phi^{(J_c)\pm}_{K_ZJK_Z}(\{\boldsymbol{Z}_j, \xi_j\})|\Phi^{(J_c)\pm}(\{\boldsymbol{Z}_j, \xi_j\})\rangle}{\|\Phi^{(J_c)\pm}_{K_ZJK_Z}(\{\boldsymbol{Z}_j, \xi_j\})\|\cdot\|\Phi^{(J_c)\pm}(\{\boldsymbol{Z}_j, \xi_j\})\|}\right|^2, \\ \left|\dfrac{\langle\Phi^{(J_c)\pm}_{K_XJK_X}(\{\boldsymbol{Z}_j, \xi_j\})|\Phi^{(J_c)\pm}(\{\boldsymbol{Z}_j, \xi_j\})\rangle}{\|\Phi^{(J_c)\pm}_{K_XJK_X}(\{\boldsymbol{Z}_j, \xi_j\})\|\cdot\|\Phi^{(J_c)\pm}(\{\boldsymbol{Z}_j, \xi_j\})\|}\right|^2.\end{cases} \tag{17}$$

Comparing $a^2(J_c, J)$ for $K=K_X$ to that for $K=K_Z$, we find that $a^2(J_c, J)$ with low J is larger for $K=K_Z$ than for $K=K_X$, while $a^2(J_c, J)$ with high J ($J\geq6$) is larger for $K=K_X$ than for $K=K_Z$. Note here that the projection for $K=K_X$ is made with respect to the integration z-axis parallel to the vector $\hat{\boldsymbol{J}}$ which is the expectation value of total spin operator $\boldsymbol{J}^{\rm op}$. We see that, for a fixed J_c, $a^2(J_c, J)$ is large for $J=J_c$ and $J=J_c+2$. It decreases as J goes far away from J_c or J_c+2. An interesting fact is that $a^2(J_c, J)$ with $J=J_c+2$ is often as large as (sometimes larger than) the one with $J=J_c$

Table III. The energy expectation value of the angular-momentum-projected state $|\Phi^{(J_c)\pm}_{KJM}\rangle$. The observed binding energy of ^{20}Ne ground state is 160.65 MeV.

			$E/^c$(MeV)				
J_c^π	$\hat{E}$(MeV)		$J=0$	$J=2$	$J=4$	$J=6$	$J=8$
0^+	158.00	$K_Z=0$	163.55	162.45	159.74	154.4	144.7
0^+		$K_X=J$	163.55	162.43	159.40	153.70	143.06
2^+	156.87	$K_Z=0$	163.43	162.44	159.86	154.9	145.51
2^+		$K_X=J$	163.43	162.53	160.03	155.07	144.89
4^+	154.66	$K_Z=0$	161.03	160.33	158.51	154.93	147.48
4^+		$K_X=J$		160.31	158.62	155.16	147.63
6^+	150.66	$K_Z=0$	157.76	157.24	155.9	153.52	149.07
6^+		$K_X=J$		157.12	155.89	153.58	149.24
8^+	145.80	$K_Z=0$					146.02
8^+		$K_Z=J$					146.03

			$E/^c$(MeV)				
J_c^π	$\hat{E}$(MeV)		$J=1$	$J=3$	$J=5$	$J=7$	$J=9$
1^-	147.81	$K_Z=0$	153.25	151.09	146.85	139.94	130.58
3^-	145.48	$K_Z=0$	152.78	150.70	146.64	139.90	130.04
5^-	141.08	$K_Z=0$	151.55	149.78	146.29	140.35	130.57
7^-	134.87	$K_Z=0$	147.62	146.26	143.66	139.39	131.79
9^-	126.59	$K_Z=0$					129.23

except for the case with $J_c=8$. It is unexpected that the cranked state with the spin constraint J_c has the largest component not necessarily of the spin $J=J_c$ state but of the larger spin state $J=J_c+2$.

In Table III we show the energy expectation value of the state $|P^{J_c}_{KM}\Phi^{(J_c)\pm}(\{Z_j, \xi_j\})\rangle$ for $K=K_Z$ and K_X. Comparing the results with given (J_c, J), we have found that the energies obtained with respect to $K_Z=0$ and $K_X=J$ are almost the same. To tell in detail, the results for $K_X=J$ may be said to be slightly lower than for $K_Z=0$ when $J_c \geq 4$ and $J \geq 4$. The lower energy with given (J_c, J) is denoted by $E_J^{(J_c)\pm}$. We have compared the values $E_J^{(J_c)\pm}$ with various values for J_c within each column of the fixed value J in the Table. An interesting but unexpected fact we have found is that the lowest energy for the angular momentum J is not necessarily given by $E_J^{(J_c=J)\pm}$ but often by $E_J^{(J_c=J-2)\pm}$ as is seen in the cases $J^\pi=4^+\sim 8^+$ (see the three columns on the right side of the upper table).

The fact that $E_J^{(J_c=J-2)\pm}$ is often lower than $E_J^{(J_c=J)\pm}$ means that the rotating intrinsic state for the $J^{(\pi=\pm)}$ state is not given by $|\Phi^{(J_c=J)\pm}(\{Z_j, \xi_j\})\rangle$ but often by $|\Phi^{(J_c=J-2)\pm}(\{Z_j, \xi_j\})\rangle$. Then the structure-change from the 6^+ state to the 8^+ state should be discussed not by comparing $|\Phi^{(J_c=6)+}(\{Z_j, \xi_j\})\rangle$ with $|\Phi^{(J_c=8)+}(\{Z_j, \xi_j\})\rangle$, but by comparing $|\Phi^{(J_c=4)+}(\{Z_j, \xi_j\})\rangle$ with $|\Phi^{(J_c=6)+}(\{Z_j, \xi_j\})\rangle$. Since the intrinsic state $|\Phi^{(J_c=6)+}(\{Z_j, \xi_j\})\rangle$ has the $^{16}O+\alpha$ clustering feature although not so prominent, the structure-change from the 6^+ state to the 8^+ state would be regarded as being not so drastic as one would expect from the change between $|\Phi^{(J_c=6)+}(\{Z_j, \xi_j\})\rangle$ and $|\Phi^{(J_c=8)+}(\{Z_j, \xi_j\})\rangle$.

We show in Fig. 5 the comparison of $E_J^{(J_c=J)\pm}$ with the lowest value of the energy $E_J^\pm$ for each angular momentum J. In this figure we also show the observed energy spectra of the ground band and the negative parity band upon 5.78 MeV 1^- state. We see that the reproduction of the observed energy spectra of the ground band by the theoretical spectra of E_J^+ is good. Especially the observed shrinkage of the energy interval between 6^+ and 8^+ is fairly well reproduced by the theory, while the $^{16}O+\alpha$ cluster model has been unsuccessful in reproducing this energy shrinkage.

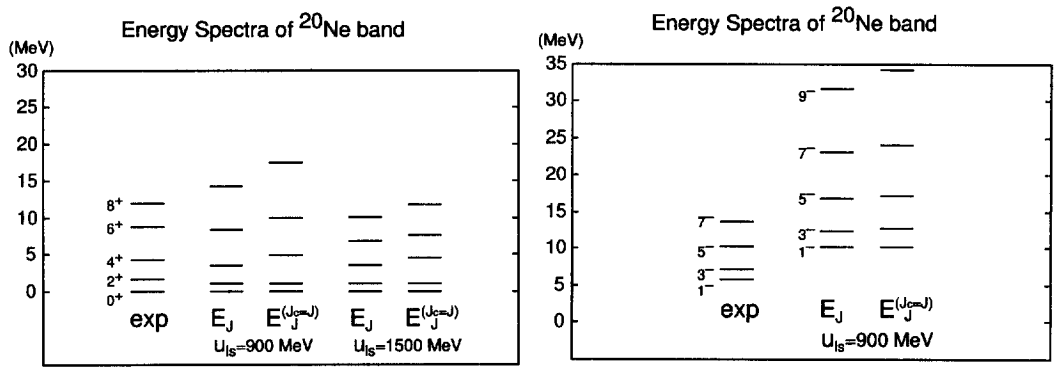

(a) (b)

Fig. 5. The energy of the angular momentum projected state. E^{J^c} stands for the energy of the state with angular momentum J obtained by projection from the intrinsic state with the constraint J_c, while E_J stands for the minimum value of E^{J^c} with fixed J among possible J_c values.

As for the negative parity rotational band, however, as seen in Fig. 5, the present calculation is not satisfactory in reproducing energy spectra in two points. The first point is the larger gap energy than data between this negative parity band and the ground band. The second point is the smaller moment of inertia than data, which causes the level spacings between adjacent band members wider than data. Both of these points indicate that the distance between the α cluster and the ^{16}O cluster should be larger than the present calculation. Therefore the following three kinds of modifications and improvements will be the next step of investigation to be done in future in order to get better reproduction of the energy spectra: The first is to adopt slightly stronger Majorana exchange mixture m than the present value of $m=0.6$, because it makes the clustering feature more prominent resulting in the smaller gap energy between the inversion doublet bands. The second is to introduce the density-dependent force into the two-nucleon central force, because it gives larger energy gain to the negative parity band due to its more dilute density than the positive parity band. The third is to superpose the AMD determinants so that the α-^{16}O relative wave function has longer tail in the outer spatial region. It is because the negative parity band is expected to have longer tail than the positive parity band.

The excitation energies without the angular momentum projection are 0, 1.22, 3.54, 8.06, 14.95, 29.98, 45.92 MeV for $L_c^\pi=0^+, 2^+, \cdots, 10^+, 12^+$ and 10.01, 12.34, 16.74, 22.95, 31.23, 43.16 MeV for $L_c^\pi=1^-, \cdots, 9^-, 11^-$, respectively. Simple cranked states with the orbital angular momentum constraint L_c higher than 10 shows the higher excitation energies than the ones expected from the rotating energy rule of $J(J+1)$.

4.5. *Dependence on the spin-orbit force*

We have already seen in § 4.3 that the magnitude of $\hat{S}$ is exceptionally large in $|\Phi^{(J_c=8)+}(\{Z_j, \xi_j\})\rangle$, while it is very small in other rotating intrinsic states with $J_c \leq 6$. Therefore it is expected that the energy $E^{J_c=8)+}_{J=8}$ can depend more strongly on the strength of the two-body spin-orbit force than the energy $E^{J_c=6)+}_{J=8}$. More generally speaking, the energy of a state with dissolved clusters can depend strongly on the two-body spin-orbit force. This also means that the degree of the cluster dissolution in the rotating intrinsic state can depend on the spin-orbit force. In order to investigate the structure-change from 6^+ to 8^+ slightly in more detail, we have studied whether the increase of the strength of the two-body spin-orbit force changes appreciably or not the result on the structure-change from 6^+ to 8^+ obtained with the present value $u_I = -u_{II} = 900$ MeV.

We have investigated the states with the constraints $J_c^\pi=0^+\sim 8^+$ adopting the increased strength $u_{ls} \equiv u_I = -u_{II} = 1500$ MeV for the spin-orbit force instead of the strength of 900 MeV. The characteristic features about the existence of clusters in the rotating intrinsic states are found to be very similar to the results with $u_{ls}=900$ MeV. Namely the intrinsic states with low J_c have α and ^{16}O clusters between which the distance becomes smaller as the angular momentum constraint value J_c increases ending with the $J_c^\pi=8^+$ state which has no recognizable cluster like an α cluster.

However discussing in more detail, we should point out that the weakening of the clustering along the increase of J_c value is more drastic than in the results with $u_{ls}=900$ MeV. An example is the change of the anti-stretching effect. We have found

that the distance between α and ^{16}O clusters is smaller than that in the case of 900 MeV for the intrinsic states with the same constraint value J_c ($J_c \leq 6$). In the state with $J_c=6$ the distance is about 2 fm in the case $u_{ls}=900$ MeV, while in case of $u_{ls}=1500$ MeV it is about 1 fm which is too small to be considered as "the well-developed α cluster". Correspondingly to it, the quadrupole moment of the latter state is smaller than that of the former state. Another effect which shows the weakening of the clustering is the dissolution of α cluster, which is seen clearly in the comparison of the expectation value of $|\hat{S}|$ in Fig. 3. $|\hat{S}|$ becomes large with increasing J_c in much more drastic way than in the case of $u_{ls}=900$ MeV.

We have studied the energy expectation value $E_J^{(J_c)+}$ which is given by the projected state $|\Phi_{KJM}^{(J_c)+}(\{Z_j, \xi_j\})\rangle$ for $u_{ls}=1500$ MeV. We show the energies $E_J^{(J_c=J)+}$ and $E_J^{(J_c=J-2)+}$ also in Fig. 5. As is expected, the energy of the state with higher spin depends more strongly on the spin-orbit force. The attractive effect of the spin-orbit force contributes so much to the energy of $|\Phi_{KJM}^{(J_c=8)+}(\{Z_j, \xi_j\})\rangle$ with no clustering structure, that $E_{=8}^{(J_c=8)+}$ with $u_{ls}=1500$ MeV becomes much lower than that with $u_{ls}=900$ MeV. In the case of the constraint $J_c^{\pi}=6^+$ the stronger spin-orbit force of $u_{ls}=1500$ MeV dissolves the clusters in $|\Phi^{(J_c=6)+}(\{Z_j, \xi_j\})\rangle$ so that $E_{=8}^{(J_c=6)+}$ with $u_{ls}=1500$ MeV becomes also lower than that with $u_{ls}=900$ MeV, although the effect is less than $E_{=8}^{(J_c=8)+}$. Since the difference between $E_{=8}^{(J_c=6)+}$ and $E_{=8}^{(J_c=8)+}$ is only 1.7 MeV, it is natural to consider that the better intrinsic state for the lowest 8^+ state is the mixed state of $|\Phi^{(J_c=6)+}(\{Z_j, \xi_j\})\rangle$ and $|\Phi^{(J_c=8)+}(\{Z_j, \xi_j\})\rangle$. Here, however, we give a comment that the squared overlap amplitude between the states $|\Phi_{KJM}^{(J_c=8)+}(\{Z_j, \xi_j\})\rangle$ and $|\Phi_{KJM}^{(J_c=6)+}(\{Z_j, \xi_j\})\rangle$ is rather large. It is 93 % for $u_{ls}=1500$ MeV while it is 75 % for $u_{ls}=900$ MeV. The calculation with $u_{ls}=1500$ MeV may be regarded as reproducing better the energy spectra especially the small excitation energy of the 8^+ state which has been difficult to reproduce in terms of cluster models.

4.6. *B(E2) values*

The $E2$ transitions within positive parity states have been calculated and compared with experiments. The calculations using the angular momentum projected wave functions have been made by performing three dimensional numerical integrations. Here we use the wave functions $|\Phi_J^{(J_c=J-2)+}(\{Z_j, \xi_j\})\rangle$ which is projected from the intrinsic state with the constraint $J_c=J-2$ for the spin J state. Here it should be stressed that we do not use any effective charge. The calculated values of $B(E2; J^+ \to (J-2)^+)$ normalized by the calculated $B(E2; 2^+ \to 0^+)$ are compared in Table IV.

Table IV. The E2 transition strength of positive parity states. They are normalized by the strength of $2 \to 0$ transition. $B(E2; J \to J-2)$ is calculated with the matrix elements between $\Phi_J^{(J_c=J-2)+}$ and $\Phi_{J-2}^{(J_c=J-4)+}$.

TRANSITION	EXP.	$B(E2)/B(E2; 2\to 0)$ THEORY	
		$u_{ls}=900$ MeV	$u_{ls}=1500$ MeV
$2\to 0$	1	1	1
$4\to 2$	1.2 ± 0.15	1.28	1.33
$6\to 4$	1.15 ± 0.15	1.20	1.00
$8\to 6$	0.4 ± 0.15	0.71	0.45

We see good reproduction of data except for $8^+ \to 6^+$ by both calculations adopting $u_{ls}=900$ MeV and 1500 MeV. The observed small $E2$ transition $8^+ \to 6^+$ has been considered to be due to the structure change from 6^+ to 8^+. The small $E2$ transition is well reproduced by the calculation with the strength of spin-orbit force $u_{ls}=1500$ MeV, while in the calculation with $u_{ls}=900$ MeV it is larger due to the small change of intrinsic structure from 6^+ state to 8^+ state.

The calculated absolute value of $B(E2; 2^+ \to 0^+)$ is 22 $e^2 \cdot fm^4$ which is much smaller than the experimental data 57 $e^2 \cdot fm^4$. The absolute value of $E2$ transition is much sensitive to interaction. We found that the calculation with the Majorana parameter $m=0.65$ gives 40 $e^2 \cdot fm^4$. It should be also taken into account that in a simple AMD framework the relative wave function between the clusters is necessarily of the form of a Gaussian packet. In the system with well-developed clusters, inter-cluster relative wave function may have a long tail in the outer spatial region which may be sensitively reflected in the electric properties such as $E2$ transition. Therefore we have improved the AMD wave function by superposing several AMD wave functions. The AMD wave functions to be superposed have been constructed by adopting the following changes of the original $\{\boldsymbol{Z}\}$ values,

$$\boldsymbol{Z}_j \to \boldsymbol{Z}_j + \frac{16}{20}\sqrt{\nu}\,\boldsymbol{C} \qquad \text{for} \qquad j=1\sim 4\,,$$

$$\boldsymbol{Z}_j \to \boldsymbol{Z}_j - \frac{4}{20}\sqrt{\nu}\,\boldsymbol{C} \qquad \text{for} \qquad j=5\sim 20\,,$$

where $\boldsymbol{Z}_1 \sim \boldsymbol{Z}_4$ are the centers of single particle wave function composing an α cluster. These AMD wave functions having several different values for the relative distance between two clusters α and ^{16}O have been all projected onto the eigenstates of angular momentum and have been superposed by diagonalizing the Hamiltonian. The resulting improved AMD wave function with Majorana parameter $m=0.65$ has proved to give the strength of $B(E2; 2^+ \to 0^+)$ as 64 $e^2 \cdot fm^4$ which somewhat overestimates data. A choice of slightly smaller value for the Majorana parameter m will give much better agreement with data.

§ 5. Summarizing discussion

In this paper we have studied, by using the AMD theory, the formation and dissolution of clusters in the yrast line states of ^{20}Ne. The reason why we have used AMD is that AMD is a theory free from any model assumptions and hence does not assume the existence of any clusters at all.

The calculated results have shown that for both positive and negative parity low spin constraints $|\langle \boldsymbol{J}^{op} \rangle| = J_c$, the two-cluster structure of $^{16}\mathrm{O}+\alpha$ constitutes a predominant configuration of the rotating (cranked) intrinsic states but this clustering becomes weaker as the spin goes up. It has been shown that the rotating intrinsic states with the constraints $J_c^{\pi}=8^+$ and 9^- are not prolate in shape and α clustering is not recognizable. Furthermore the rotating intrinsic states with the constraints $J_c^{\pi}=10^+$, 12^+ and 11^- have been found to have the three-cluster-like structure

of $C^{12}+\alpha+\alpha$.

In order to check the reliability of the above results on the structure change in the case of positive parity states, we have made an extended AMD calculation by adopting a superposition of two Slater determinants. In this calculation, for the sake of simplicity, we have fixed the nucleon spin orientations like for negative parity states. Corresponding to this simplification, the angular momentum constraint has been made not for $|\langle \boldsymbol{J}^{\rm op}\rangle|$ but for $|\langle \boldsymbol{L}^{\rm op}\rangle|$. We express $|\Phi^+(\{\boldsymbol{Z}_j, \xi_j\}, \{\boldsymbol{Z}'_j, \xi'_j\}, C)\rangle$, $|\Phi^+(\{\boldsymbol{Z}_j, \xi_j\})\rangle$ and $C|\Phi^+(\{\boldsymbol{Z}'_j, \xi'_j\})\rangle$ in Eq. (11) as Φ, Φ_I and Φ_{II}, respectively ($\Phi=\Phi_I+\Phi_{II}$). We have found that Φ_I is very similar to the AMD wave function obtained by the AMD calculation adopting a single Slater determinant and is a main component of Φ and that Φ_{II} is a small component giving only a small modification to Φ_I. We give in Table V the squared amplitude β^2 of the main component $\Phi_I/\|\Phi_I\|$ in $\Phi/\|\Phi\|$;

Table V. The squared amplitude of main component in total wave function in the extended AMD calculation.

J_c^π	β^2
0^+	1.00
2^+	0.94
4^+	0.94
6^+	0.94
8^+	0.90

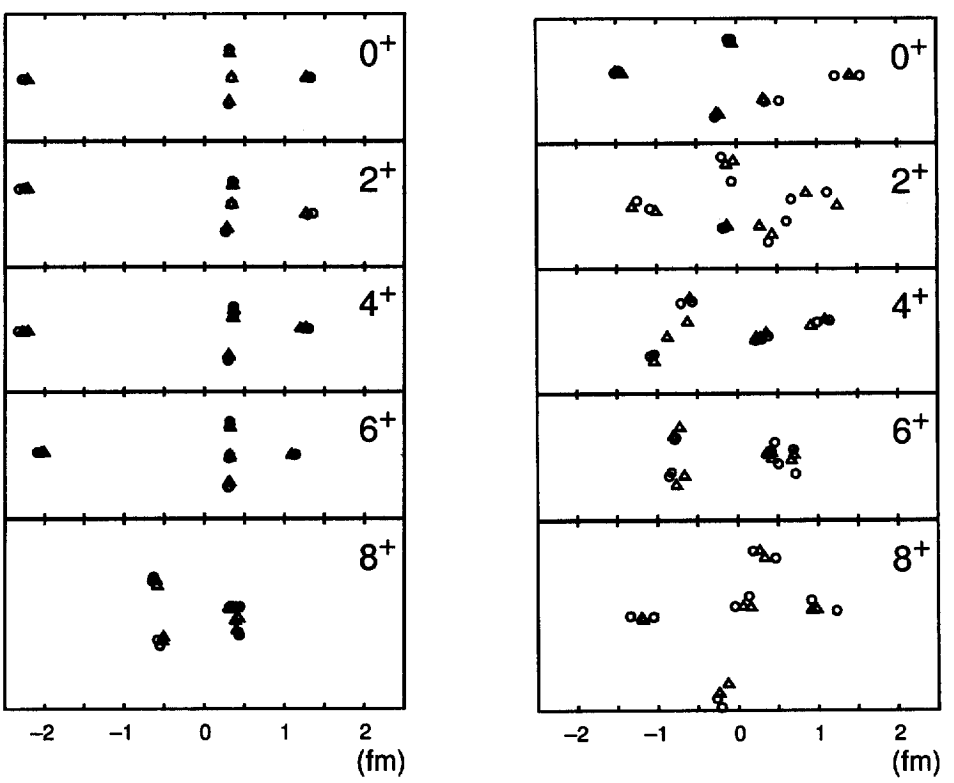

Fig. 6. The spatial centers of nucleon wave packets in the extended AMD wave function $\Phi^+=\Phi_I{}^+ + \Phi_{II}^+$. The left column is for $\Phi_I{}^+$ which is the main component while the right column is for Φ_{II}^+ which is the minor component.

$$\beta^2 \equiv \left| \frac{\langle \Phi_I | \Phi \rangle}{\| \Phi_I \| \cdot \| \Phi \|} \right|^2 . \tag{18}$$

These results give us a very clear evidence of the high reliability of the AMD method in which only one Slater determinant is adopted. We show in Fig. 6 the real parts of $\{Z_j\}$ of both Φ_I and Φ_{II}. We see that for the constraints $J_c^\pi = 0^+$, 2^+ and 4^+, Φ_{II} acts so that the thin density spatial part between α cluster and ^{16}O cluster in Φ_I becomes slightly thicker in density but that for $J_c^\pi = 6^+$ and 8^+, Φ_{II} has the three-cluster-like configuration of $^{12}\mathrm{C}+\alpha+\alpha$.

The rotating intrinsic state $|\Phi^{(J_c=8)+}(\{Z_j, \xi_j\})\rangle$ with $J_c^\pi = 8^+$ is especially interesting because we have found that it is different from other positive parity intrinsic states $|\Phi^{(J_c)+}(\{Z_j, \xi_j\})\rangle$ with $J_c \leq 6$ in two ways. One is its oblate shape and the other is its large value of $|\langle S^{\mathrm{op}} \rangle|$, both of which means the dissolution of the α cluster in this intrinsic state with $J_c = 8$. The former property has been found to persist even when the two-body spin-orbit force is switched off. Furthermore as is seen in Fig. 5, the oblate shape property of the intrinsic state with $J_c = 8$ persists even if two Slater determinants are superposed to express the intrinsic state.

The rotating intrinsic states are not eigenstates of angular momentum. Hence the good angular momentum states have been constructed by applying the projection from the rotating intrinsic states. An interesting but unexpected finding obtained by this projection calculation is that the rotating intrinsic state $|\Phi^{(J_c)\pm}(\{Z_j, \xi_j\})\rangle$ cannot necessarily be considered to express the intrinsic state of the yrast state with the angular momentum $J = J_c$. It is because the calculations within the range $0 \leq J, J_c \leq 9$ have shown that in many cases the projected state $|\Phi^{(J_c)\pm}_{KJM}(\{Z_j, \xi_j\})\rangle$ with $J_c = J$ has higher energy than the projected state $|\Phi^{(J_c)\pm}_{KJM}(\{Z_j, \xi_j\})\rangle$ with $J_c = J-2$, namely $E_J^{(J_c=J-2)\pm} < E_J^{(J_c=J)\pm}$. We have to regard that in many cases the rotating intrinsic state for the $J^{(\pi=\pm)}$ state is given rather by $|\Phi^{(J_c=J-2)\pm}(\{Z_j, \xi_j\})\rangle$. Thus the structure of the band terminal state with $J^\pi = 8^+$ should be regarded as being represented better by $|\Phi^{(J_c=6)+}(\{Z_j, \xi_j\})\rangle$ in the level of the present calculation, which means that the $J^\pi = 8^+$ state still possesses the $^{16}\mathrm{O}+\alpha$ clustering nature although not so prominent.

We study the reason of $E_J^{(J_c=J-2)\pm} < E_J^{(J_c=J)\pm}$ below. We recall the following well-known fact on the coupling of states. Let intrinsic wave functions Φ^A and Φ^B represent states A and B, respectively. The intrinsic energies E^A and E^B of Φ^A and Φ^B are close to each other but the deformation of Φ^A is much larger than that of Φ^B. In this situation, the coupling of the states A and B cannot be described by diagonalizing the Hamiltonian with Φ^A and Φ^B. If we make this diagonalization, Φ^A and Φ^B will mix appreciably with each other because E^A and E^B are close to each other and one may think that the states A and B mix strongly. But it does not represent the real situation. In order to represent the states A and B correctly, we have to use the angular momentum projected states $P^J_{MK}\Phi^A$ and $P^J_{MK}\Phi^B$ instead of the intrinsic states Φ^A and Φ^B. Since the deformation of Φ^A is much larger than that of Φ^B, the energy of the projected state $P^J_{MK}\Phi^A$ is much lower than that of $P^J_{MK}\Phi^B$. This means the coupling of $P^J_{MK}\Phi^A$ and $P^J_{MK}\Phi^B$ is small, namely the coupling of the states A and B is small.

In our present case of the band terminal state of $J^\pi = 8^+$, the $^{16}\mathrm{O}+\alpha$ clustering state

and the oblate spin-aligned shell-model state exist in a similar energy region. Since the rotating intrinsic state $|\Phi^{(J_c=8)+}(\{Z_j, \xi_j\})\rangle$ has proved to be largely of oblate spin-aligned structure, we can conjecture that the intrinsic state of $^{16}O+\alpha$ clustering has the energy close to but slightly higher than the energy of the oblate spin-aligned shell-model intrinsic state. These two intrinsic states are expected to mix resulting in the state which resembles more to the shell-model state than to the clustering state. If this is the case, by recalling the above-mentioned argument, we can expect that after the angular momentum projection the mixing between the clustering state and the shell-model state is no more large and the clustering state appears with lower excitation energy. If the intrinsic state of $^{16}O+\alpha$ clustering contained in $|\Phi^{(J_c=8)+}(\{Z_j, \xi_j\})\rangle$ is not so much different from $|\Phi^{(J_c=6)+}(\{Z_j, \xi_j\})\rangle$, it is quite reasonable to get the result $E^{J_c=6)+}_{J=8} < E^{J_c=8)+}_{J=8}$.

Similarly we can understand rather naturally the result $E_J{}^{(J_c=J-2)+} < E_J{}^{(J_c=J)+}$ for lower spin cases with $J \leq 6$. Here an important factor in yielding this result is the anti-stretching character of the rotating intrinsic state. This anti-stretching character assures the larger lowering of the energy by the angular momentum projection from $|\Phi^{(J_c=J-2)+}(\{Z_j, \xi_j\})\rangle$ than from $|\Phi^{(J_c=J)+}(\{Z_j, \xi_j\})\rangle$.

The coupling of the $^{16}O+\alpha$ clustering state and the oblate spin-aligned shell-model state in the $J^\pi=8^+$ state, of course, can change largely if the energy of the shell-model state can have much lower energy than the present value. Since we found that the magnitude of $|\langle S^{op}\rangle|$ is exceptionally large in $|\Phi^{(J_c=8)+}(\{Z_j, \xi_j\})\rangle$, we expected that the increase of the strength of the two-body spin-orbit force might lower largely the energy of the oblate spin-aligned shell-model state, while it does not affect so much the energy of the $^{16}O+\alpha$ clustering state because S^{op} has vanishing value for this clustering state. We have actually found that weakening of the clustering structure in $|\Phi^{(J_c)+}(\{Z_j, \xi_j\})\rangle$ with higher J_c is more prominent in the calculation with the stronger spin-orbit force. The structure change from 6^+ state to 8^+ state has proved to be largely more prominent in the case $u_{ls}=1500$ MeV than in the case $u_{ls}=900$ MeV, which is clearly reflected in two kinds of observables: One is the magnitude of the ratio $B(E2; 8^+ \to 6^+)/B(E2; 2^+ \to 0^+)$ and the other is the energy spacing between 6^+ and 8^+ states. The magnitudes of both quantities are much smaller for $u_{ls}=1500$ MeV than for $u_{ls}=900$ MeV and the magnitudes for $u_{ls}=1500$ MeV are closer to data.

Our present method to construct wave functions with good angular momentum variationally is the so-called projection after variation. The reason to adopt this approach is of course because the variation after projection by the use of the AMD wave function is not easy to make numerically. Our finding that in many cases we had better regard $|\Phi^{(J_c)\pm}(\{Z_j, \xi_j\})\rangle$ as the intrinsic state of the yrast state with the angular momentum $J=J_c+2$ rather than that with $J=J_c$ is just coming from the fact that the projection after variation is sometimes insufficient. This defect is common to all the approaches adopting the idea of cranking constraint in constructing the intrinsic states, which include the cranked cluster model[33),34)] and the mean field theories such as the cranked Nilsson model and the cranked Hartree-Fock method. Since in our approach we always make the angular momentum projection, it is more reasonable to regard $|\Phi^{(J_c)\pm}(\{Z_j, \xi_j\})\rangle$ as a trial function with the continuous var-

iational parameter J_c not taking only integer values.

Finally we compare our cranked AMD approach with the cranked Hartree-Fock method. We consider that the AMD approach has the following three kinds of advantage over the cranked Hartree-Fock method. The first point is that the AMD is completely free from any model assumptions. In principle, Hartree-Fock calculations can be made without any model assumptions. However, in actual calculations, completely unrestricted Hartree-Fock calculations are too difficult to perform and many restrictions have to be introduced such as the assumption of the axial symmetric deformation and the truncation of high $\hbar\omega$ orbitals in the expansion of single particle wave functions. The second point is that the AMD calculation can be easily performed and have been actually performed by adopting a linear combination of Slater determinants (avoiding any model assumptions at all). In this sense, the AMD approach is far advanced beyond the Hartree-Fock approach. The third point is that the cranking condition can be imposed very satisfactorily in the AMD. Namely, in the AMD there is no a priori assumption of nuclear shape and hence the constraint is put only on the magnitude of the angular momentum while the direction of the angular momentum is determined by the energy variation. It is in a sharp contrast to the usual approach of the cranked Hartree-Fock method where the axially symmetric deformation is assumed a priori and the direction of the angular momentum vector is chosen from the outset to be parallel to the principal axis. In our present study, we have found that in most states the angular momentum vector $\hat{\boldsymbol{J}}=\langle \boldsymbol{J}^{\mathrm{op}} \rangle$ is parallel to the principal X-axis with the largest moment of inertia, but in some cases $\hat{\boldsymbol{J}}$ is tilted from the X-axis. It is a future task to make analyses of the direction of $\hat{\boldsymbol{J}}$.

Acknowledgements

The authors would like to thank Mr. A. Ono and Dr. T. Nakatsukasa for discussions and for the help in numerical calculations. The computer calculation for this work was supported in part by Research Center for Nuclear Physics (RCNP), Osaka University.

References

1) *Proc. V Int. Conf. Clustering Aspects in Nuclear and Subnuclear Systems, Kyoto, 1988*, ed. K. Ikeda, K. Katori and Y. Suzuki [J. Phys. Soc. Jpn. Suppl. **58** (1989)].
2) *Proc. IV Int. Conf. Clustering Aspects of Nuclear Structure and Nuclear Reactions, Chester, 1984*, ed. J. S. Lilley and M. A. Nagarajan (Reidel, Dordrecht, 1985).
3) K. Ikeda, H. Horiuchi, S. Saito, Y. Fujiwara, M. Kamimura, K. Kato, Y. Suzuki, E. Uegaki, H. Furutani, H. Kanada, T. Kaneko, S. Nagata, H. Nishioka, S. Okabe, T. Sakuda, M. Seya, Y. Abe, Y. Kondo, T. Matsuse and A. Tohsaki-Suzuki, Prog. Theor. Phys. Suppl. No. 68, (1980).
4) A. Arima, in *Heavy Ion Collisions,* ed. R. Bock (North Holland, Amsterdam, 1979), Vol. 1, Chap. 3, p. 417.
5) Y. C. Tang, *Lecture Notes in Physics* **145** (Springer, Berlin, 1981).
6) V. I. Kukulin, V. G. Neudatchin, I. T. Obukhovski and Yu. F. Smirnov, *Clustering Phenomena in Nuclei* (Vieweg, Braunschweig, 1982), Vol. 3, p. 1.
7) H. Horiuchi and K. Ikeda, in *International Review of Nuclear Physics*, ed. T. T. S. Kuo and E. Osnes (World Scientific, Singapore, 1985), Vol. 4, p. 1.
8) K. Ikeda, N. Takigawa and H. Horiuchi, Prog. Theor. Phys. Suppl. Extra Number (1968), 464.
9) H. Horiuchi, K. Ikeda and Y. Suzuki, Prog. Theor. Phys. Suppl. No. 52 (1972), 89.
10) H. Horiuchi and K. Ikeda, Prog. Theor. Phys. **40** (1968), 277.

11) F. Nemoto, Y. Yamamoto, H. Horiuchi, Y. Suzuki and K. Ikeda, Prog. Theor. Phys. **54** (1975), 104.
12) M. Kamimura, T. Matsuse and K. Takada, Prog. Theor. Phys. **47** (1972), 1537.
13) T. Matsuse, M. Kamimura and Y. Fukushima, Prog. Theor. Phys. **53** (1975), 706.
14) T. Inoue, T. Sebe, H. Hagiwara and A. Arima, Nucl. Phys. **59** (1964), 1.
Y. Akiyama, A. Arima and T. Sebe, Nucl. Phys. **A138** (1969), 273.
A. Arima, M. Sakakura and T. Sebe, Nucl. Phys. **A170** (1971), 273.
15) T. Tomoda and A. Arima, Nucl. Phys. **A303** (1978), 217.
16) A. Arima, H. Horiuchi, K. Kubodera and N. Takigawa, in *Advances in Nuclear Physics*, ed. M. Baranger and E. Vogt (Plenum, New York, 1972), Vol. 5, Chap. 3, p. 345.
17) Y. Fujiwara, H. Horiuchi and R. Tamagaki, Prog. Theor. Phys. **61** (1979), 1629.
18) R. Middleton, J. D. Garrett and H. T. Fortune, Phys. Rev. Lett. **27** (1971), 950.
19) L. R. Greenwood, R. E. Segel, K. Raghunathan, M. A. Lee, H. T. Fortune and J. R. Erskine, Phys. Rev. **C12** (1975), 156.
20) K. Nagatani, M. J. Le Vine, T. A. Belote and A. Arima, Phys. Rev. Lett. **27** (1971), 1071.
21) H. Horiuchi, Nucl. Phys. **A522** (1991), 257c.
22) H. Horiuchi, T. Maruyama, A. Ohnishi and S. Yamaguchi, in *Proc. Int. Conf. on Nuclear and Atomic Clusters, Turku, 1991*, ed. M. Brenner, T. Lönnroth and F. B. Malik (Springer, 1992), p. 512; in *Proc. Int. Symp. on Structure and Reactions of Unstable Nuclei, Niigata, 1991*, ed. K. Ikeda and Y. Suzuki (World Scientific, 1992), p. 108.
23) H. Horiuchi, A. Ono, Y. Kanada, T. Maruyama and A. Ohnishi, in *Proc. First Joint Italian-Japanese Meeting within the INFN-RIKEN Agreement on Perspectives in Heavy Ion Physics, Catania, 1992*, ed. M. Di Toro and E. Migneco [Italian Physical Society Conference Proceedings Vol. 38 (1993), p. 223].
24) A. Ono, H. Horiuchi, T. Maruyama and A. Ohnishi, Phys. Rev. Lett. **68** (1992), 2898.
25) A. Ono, H. Horiuchi, T. Maruyama and A. Ohnishi, Prog. Theor. Phys. **87** (1992), 1185.
26) A. Ono, H. Horiuchi, T. Maruyama and A. Ohnishi, Phys. Rev. **C47** (1993), 2652.
27) A. Ono, H. Horiuchi and T. Maruyama, Phys. Rev. **C48** (1993), 2946.
28) H. Feldmeier, Nucl. Phys. **A515** (1990), 147; in *Proc. NATO Advanced Study Institute on the Nuclear Equation of State, Peñiscola, 1989*, ed. W. Greiner and H. Stöcker (Plenum, 1989), p. 375.
29) D. M. Brink, in *Proc. Int. School of Phys. "Enrico Fermi", course 36*, ed. C. Bloch (1965), p. 247.
30) S. Drożdż, J. Okolowcz and M. Ploszajczak, Phys. Lett. **109B** (1982), 145.
E. Caurier, B. Grammaticos and T. Sami, Phys. Lett. **109B** (1982), 150.
W. Bauhoff, E. Caurier, B. Grammaticos and M. Ploszajczak, Phys. Rev. **C32** (1985), 1915.
31) A. B. Volkov, Nucl. Phys. **74** (1965), 33.
32) N. Yamaguchi, T. Kasahara, S. Nagata and Y. Akaishi, Prog. Theor. Phys. **62** (1979), 1018.
R. Tamagaki, Prog. Theor. Phys. **39** (1968), 91.
33) H. Horiuchi, T. Wada and K. Yabana, Prog. Theor. Phys. **76** (1986), 837.
34) E. Caurier and B. Grammaticos, J. of Phys. **G9** (1983), L125.
W. D. M. Rae and S. Marsh, Phys. Lett. **161B** (1985), 251.